

Catalysis Science & Technology

Accepted Manuscript



This is an *Accepted Manuscript*, which has been through the Royal Society of Chemistry peer review process and has been accepted for publication.

Accepted Manuscripts are published online shortly after acceptance, before technical editing, formatting and proof reading. Using this free service, authors can make their results available to the community, in citable form, before we publish the edited article. We will replace this *Accepted Manuscript* with the edited and formatted *Advance Article* as soon as it is available.

You can find more information about *Accepted Manuscripts* in the [Information for Authors](#).

Please note that technical editing may introduce minor changes to the text and/or graphics, which may alter content. The journal's standard [Terms & Conditions](#) and the [Ethical guidelines](#) still apply. In no event shall the Royal Society of Chemistry be held responsible for any errors or omissions in this *Accepted Manuscript* or any consequences arising from the use of any information it contains.

Enhanced visible light driven photoelectrocatalytic oxidation of ethanol at reduced graphene oxide/CdS nanowires decorated with Pt nanoparticles

Abbas Arabzadeh,^a Abdollah Salimi,^{a,b} Maysam Ashrafi,^a Saeid Soltanian^c*

and Peyman Servati^c

^a Department of Chemistry, University of Kurdistan, 66177-15175 Sanandaj, Iran

^b Research Center for Nanotechnology, University of Kurdistan, 66177-15175 Sanandaj, Iran

^c Department of Electrical and Computer Engineering, University of British Columbia, 2332 Main Mall, Vancouver, BC V6T 1Z4, Canada

ABSTRACT: In this study, we reported the preparation of a novel ternary hybrid consisting of reduced graphene oxide/CdS nanowires decorated with Pt nanoparticles (rGO/CdS NWs/Pt NPs) as an efficient electrocatalytic and photoelectrocatalytic ethanol oxidation platform in alkaline media. The synthesis was accomplished by a solvothermal method in the first step to prepare uniformly sized CdS NWs with diameters of 35 nm and lengths up to several micrometers, followed by a simple hydrothermal method to assemble CdS NWs decorated Pt NPs onto rGO sheets using hydrazine as reducing agent. The data regarding the morphology, structure and properties of prepared nanocomposite were obtained through various characterization techniques including field-emission scanning electron microscopy (FESEM), transmission electron microscopy (TEM), energy dispersive X-ray spectroscopy (EDX), X-ray diffraction (XRD), X-ray photoelectron spectroscopy (XPS), UV-visible and photoluminescence Spectroscopy (PL). Assessing the electrocatalytic activity using cyclic voltammetry (CV) and amperometry techniques revealed that the ternary hybrid (rGO/CdS NWs/Pt NPs) exhibited superior electrocatalytic activity toward ethanol oxidation in alkaline solution with more negative onset potential compared to various component nanostructures of CdS NWs, rGO/CdS NWs, CdS NWs/Pt NPs and rGO/Pt NPs. Furthermore, experiments using low power LED as visible-light illumination source showed a dramatic increase in electrocatalytic activity of proposed nanohybrid toward ethanol oxidation accompanied by a shift of onset potential to more negative potential of -0.950 V *vs.* Ag/AgCl compared to -0.870 V in dark condition. This high electrocatalytic and photoelectrocatalytic performance can be ascribed to providing maximum interfacial contact of CdS NWs with rGO, which decrease the agglomeration of nanostructures

and suppress the photogenerated electron-hole recombination. Furthermore, accelerated electron transfer in the presence of rGO and enhanced specific surface area achieved by uniform deposition of Pt NPs onto CdS NWs contribute in increasing the catalytic activity. This research could promise a simple strategy toward synthesis of one-dimensional semiconductor-rGO/Pt ternary hybrid and its applications as an efficient visible-light photocatalyst for different chemical transformations and energy conversions devices.

INTRODUCTION

Development of direct alcohol fuel cells (DAFCs) has been widely studied to convert their stored chemical energy into electrical energy with high utilization efficiency and low polluting emissions.^{1,2} Ethanol is a promising fuel in the DAFCs due to low toxicity, high boiling point for safe storage in transportation applications, the nature of 12-electron transfer upon complete oxidation, which results in its higher energy density (8 kWh kg⁻¹) compared to methanol (6.09 kW·h kg⁻¹) and formic acid (1.740 kW·h kg⁻¹), and also being a green and renewable resource which can be easily produced from agricultural products or biomass in a large scale.³⁻¹¹ In particular, direct ethanol alkaline fuel cells (DEAFCs) have attracted much interest in recent years.⁵⁻¹¹ Alkaline electrolytes offer unique properties for efficient ethanol electrooxidation, such as the enhanced electrochemical kinetics at low anodic overpotential and the lowered risk of corrosion of materials for long-term applications, reduced fuel crossover from the anode to the cathode via electro-osmotic drag of hydrated hydroxyl ions, and the possibility of using both precious and non-precious metal catalysts.⁵⁻¹¹

It is well-known that Pt and its alloys are among the most efficient electrocatalysts in the anodic oxidation of fuels, due to their excellent properties in the adsorption and dissociation of small organic molecules such as ethanol and methanol.^{9,12,13} However, high amount of Pt usage and its high cost nature are main issues that need to be addressed in energy conversion field. In this respect, loading the Pt catalyst particles on suitable carriers has been a choice extensively pursued by many researchers in order to achieve both high catalytic performance and lower cost. Graphene, an atomic-layer-thick 2D material, with excellent conductivity, high chemical stability

and large surface area ($2600 \text{ m}^2 \text{ g}^{-1}$) is a material of choice which has been applied as promoter and catalyst support to construct highly effective electrodes for fuel cells or corrosion resistance devices.¹¹⁻¹⁷

On the other hand, great research efforts have been input over the recent years to design photoelectrocatalytic systems as alternatives to the conventional electrocatalytic processes. To date, many semiconductors including TiO_2 , WO_3 , CuO , SrTiO_3 , etc have been applied in photoelectrocatalytic reactions for energy conversion and photo-fuel-cells (PFC_S) design. Cadmium sulfide (CdS), an important semiconductor with relatively narrow band gap of 2.52 eV at room temperature, has attracted considerable interest in photocatalysis,¹⁸⁻²³ photoelectrochemical,²⁴ light-emitting diodes,²⁵ water splitting,²⁶ solar cells,^{27,28} photosynthesis²⁹ and photo-fuel-cells (PFCs).³⁰ Novel physical and chemical properties of CdS could be realized by controlling the particle sizes, microstructure of CdS or decorating with other metal nanoparticles.¹⁸ Furthermore, the stability of the CdS nanostructure improved with controlling of synthesis condition.³¹ Nonetheless, its rapid recombination rate of photogenerated electron-hole pairs and easy aggregation of CdS nanoparticles reduce the specific surface area and reactive sites, which leads to poor photoelectrocatalytic activity.³² The coupling of CdS with other wide-band gap semiconductors such as graphene oxide (GO) has been adopted to solve these drawbacks. In addition, the integration of Pt NPs onto semiconductor-graphene nanocomposites has been shown to possess superior catalytic or photocatalytic activity and larger durability for electrocatalytic oxidation of fuels or hydrogen evolution processes.^{1,32} However, CdS NPs have poor interfacial contact with the graphene surface due to the nearly spherical shape of NPs and tend to agglomerate. Therefore, preparing a form of CdS nanostructures such as CdS NWs that

provide higher interfacial contact with graphene without aggregation is a key factor to enhance the photocatalytic or photoelectrocatalytic performance of CdS-graphene nanocomposites.

On the basis of the above discussion, in this work, we have reported the synthesis of a novel ternary hybrid composed of rGO/CdS NWs decorated with Pt NPs. A simple one-step hydrothermal strategy was utilized for assembly of CdS NWs onto GO and in situ reduction of PtCl_4^{2-} and GO to form a uniformly distributed Pt NPs onto CdS NWs/rGO using hydrazine as reducing agent (Scheme 1). The prepared rGO/CdS NWs/Pt NPs nanocomposite was fully characterized by different microscopic, spectroscopic and electrochemical techniques and its electrocatalytic activity toward ethanol oxidation was evaluated in alkaline media. Control experiments were designed and performed with different single and double-hybrid nanomaterials such as CdS NWs, rGO/CdS NWs, CdS NWs/Pt NPs and rGO/Pt NPs to show the enhanced electrocatalytic performance of the proposed ternary hybrid. Furthermore, the photoelectrocatalytic activity of rGO/CdS NWs/Pt NPs nanocomposite toward ethanol oxidation was investigated under visible light illumination using low power LED as light source. Interestingly, with assistance of visible light illumination, a large potential shift toward more negative values was observed for the onset potential of ethanol oxidation, accompanied by a three-fold increase in electrocatalytic current and great improvement in the stability of photocatalyst. The exciting electrocatalytic and photoelectrocatalytic behavior of the prepared ternary hybrid demonstrating in the obtained results, has its origin in the higher interfacial contact of 1D CdS NWs with rGO, leading to decrease in the agglomeration and also, suppression of photogenerated electron-hole recombination,^{19,33} as well as the uniform distribution of Pt NPs onto CdS NWs, providing large specific surface area and thus, increase the catalytic activity.

EXPERIMENTAL SECTION

Chemicals and materials. Graphite powder, Sodium diethyldithiocarbamate trihydrate ($C_5H_{10}NNaS_2 \cdot 3H_2O$), ethylenediamine ($C_2H_8N_2$) and hydrazine (N_2H_4) were purchased from Merck (Darmstadt, Germany). Ethanol (C_2H_5OH), potassium tetrachloroplatinate (IV) (K_2PtCl_4), cadmium chloride ($CdCl_2$) and potassium hydroxide (KOH) were purchased from Sigma-Aldrich (USA). Other chemicals were of analytical grade purchased from Merck and Sigma-Aldrich. High-purity deionized (DI) water was used throughout the experiments.

Instruments and experimental techniques. The electro- and photo-electrochemical measurements were performed at room temperature with Autolab (PGSTAT30), potentiostat/galvanostat and Metrohm (Type 1.757.0010) instruments connected to a three-electrode cell, linked to a computer (Pentium IV, 1200 MHz) and the cell linked to the instrument software. A conventional three-electrode cell was used for all experiments. Modified glassy carbon (GC) electrode used as working electrode, platinum wire and Ag/AgCl/KCl (sat'd) were used as auxiliary and reference electrodes, respectively. Before each electrochemical measurement, the solution was well purged with N_2 for removing oxygen. EIS measurements were carried out in a conventional three-electrode cell, powered by an electrochemical system comprising the ZAHNER (model IM6ex, Germany). The system was run on a PC using THALES USB software. For these measurements, a frequency range of 0.1 Hz to 10 kHz was employed and the AC voltage amplitude was 5 mV. Scanning electron microscopy (SEM) images were obtained with a MIRA3 TESCAN HV: 20.0 KV (Czech Republic). UV-Vis and fluorescence spectra were recorded on a SPECTROD 250 Analytik Jena spectrophotometer (Germany) and an EL01044753-Varian spectrophotometer (USA), respectively. XRD patterns were recorded on a Bruker D8 Advance diffractometer equipped with a copper source and

a General Area Detector Diffraction System (GADDS). XPS was performed using an Omicron Nanotechnology equipped with an EA 125 Energy Analyzer and a DAR 400 X-Ray source. The TEM/STEM images were obtained using a FEI Tecnai Osiris Scanning Transmission Electron Microscope operated at 200 KV. Elemental mapping analysis was carried out by high-angle annular dark-field (HAADF) STEM EDS.

Preparation of rGO/CdS NWs/Pt NPs. GO was synthesized using a modified Hummer's method³³ with details given in supporting information (SI). The rGO/CdS NWs/Pt NPs has been fabricated by a facile template-free two-step solvothermal method, as illustrated in Scheme 1.

(a) *Synthesis of CdS NWs.* Uniform CdS NWs were grown through a modified previously reported method.^{20,34} In a typical process, 1.124g of cadmium diethyldithiocarbamate ($\text{Cd}(\text{S}_2\text{CNEt}_2)_2$), prepared by precipitation from a stoichiometric mixture of sodium diethyldithiocarbamate trihydrate and cadmium chloride in deionized water, was added to a 50-mL capacity Teflon-lined stainless steel autoclave containing 40 mL ethylenediamine. The autoclave was maintained at 180 °C for 24 h and then allowed to cool to room temperature. A yellowish precipitate (shown in Figure S1A (SI)) was collected and washed with absolute ethanol and deionized water to remove residual organic solvents. The final products of CdS NWs were dried in an oven at 60 °C.

(b) *Synthesis of rGO/CdS NWs/Pt NPs.* First, 2.5 mg of GO was well dispersed in 30 mL of distilled water by ultrasonication. Similarly, fine dispersions of 14 mg CdS NWs in 15 mL of ethanol and 6.2 mg K_2PtCl_4 in 10 mL distilled water were prepared separately with the aid of ultrasonication. Then, these solutions were well mixed together by stirring and sonication. After adding 350 μL hydrazine as reducing agent while stirring, the above solution was transferred into a 100-mL stainless steel autoclave with a Teflon liner and kept at 180 °C for 15 h. The dark

slime green precipitates (shown in Figure S1B (SI)) thus obtained were collected, washed thoroughly with deionized water and ethanol, and then dried in an oven at 60°C. The amounts of rGO and CdS NWs for synthesis of rGO/CdS NWs/Pt NPs nanocomposite were ~13% and ~72% wt, respectively. For synthesis of quantum dots/graphene nanocomposite, usage of $\geq 5\%$ rGO and $\geq 70\%$ CdS nanostructures is common.^{22,33,35,36}

For control experiments, rGO/CdS NWs, CdS NWs/Pt NPs and rGO/Pt NPs nanocomposites were also synthesized by the method as just described, but without adding the platinum salt precursor, GO and CdS NWs, respectively. To prepare the modified GC electrodes, specified amount of each composite was well dispersed in 2 ml of absolute ethanol by stirring and sonication. Then, 2 μ l of dispersed solution was placed on the electrode surface and allowed to dry at room temperature. This operation was repeated 3 times for each electrode modification.

RESULTS AND DISCUSSION

Characterization of rGO/CdS NWs/Pt NPs composite. Figure 1 shows the typical SEM images of CdS NWs and rGO/CdS NWs/Pt NPs composite. As can be seen in Figures 1A and 1B, the as-prepared CdS NWs are in the form of almost uniformly-sized individual 1D NWs with an average diameter of ca. 35 ± 3 nm and lengths 2.5 ± 0.6 μ m. Also, it is evident from Figure 1 C-E that a large quantity of small spherical Pt NPs are well distributed within the rGO/CdS NWs composite and all the outlines of CdS NWs, rGO and Pt NPs can be clearly seen. Further characterization of rGO/CdS NWs/Pt NPs nanocomposite is come from the EDX image in Figure S2 (SI) which confirms the existence of Pt, Cd, S and C elements in the composite structure.

The crystallinity of the as-prepared CdS NWs and rGO/CdS NWs/Pt NPs nanocomposite is examined by XRD and data are shown in Figure 2. Those peaks marked with “#” can be indexed

to hexagonal wurtzite CdS (PDF, 74-9663), while additional peaks denoted by “*” and “▼” correspond to the cubic Pt (PDF, 87-0636) and the (002) planes of rGO, respectively. The as-prepared CdS NWs exhibit diffraction peaks, in terms of CdS framework, in which the peaks at 2θ values of 24.8° , 26.5° , 28.2° , 36.6° , 43.7° , 47.9° , 50.9° , 51.8° , 52.8° , 58.9° , 66.8° , 69.2° , 70.9° , 72.3° , and 75.4° can be attributed to the (100), (002), (101), (102), (110), (103), (200), (112), (201), (202), (203), (210), (211) and (212) crystal planes of hexagonal wurtzite CdS (PDF, 74-9663), respectively.^{20,34} All diffraction peaks are indexed to pure CdS with hexagonal crystal structure with lattice constants of $a=0.4136$ and $c=0.6716$ nm (PDF, 74-9663). In addition, for rGO/CdS NWs/Pt NPs nanocomposite, two diffraction peaks observed at 39.4° and 46.0° correspond to (111) and (200) diffraction planes of cubic Pt with lattice constant of 0.394 nm (PDF, 87-0636), individually.³² These results are indicative of successful deposition of Pt NPs on rGO/CdS NWS composite.

TEM was also used for characterizing the structure of the synthesized CdS NWs after being decorated with Pt NPs. Figure 3 A-C reveals the uniform decoration of 3-5 nm Pt NPs on the surface of CdS NWs. To further examine the crystal structure of NWs, they were characterized by electron diffraction and High resolution TEM (HRTEM) (Figure 3D). As can be seen, the NWs are straight with almost constant diameter along the entire nanowire length. The HRTEM images and corresponding selected area electron diffraction (SAED) patterns recorded with electron beams perpendicular to the long axis of the NWs at three different positions are shown in Figure 3D a-c. The clear lattice fringes can be seen for all three positions of NWs, confirming their highly crystalline nature with interplane lattice spacing of ~ 0.335 nm parallel to the nanowire axis, corresponding to the interplane distance of (002) planes of CdS with hexagonal crystal structure. Measuring the position of sharp diffraction spots in the corresponding SAED

patterns provides further evidence to the crystalline nature of the NWs and growth along the *c*-axis.

To further investigate the composition and distribution of different elements on the nanostructure composite, elemental mapping was performed by high-angle annular dark-field (HAADF) STEM-EDS. The HRTEM with low and high magnification for rGO/CdS NWs/Pt NPs nanocomposite and elemental mapping for these cases were presented in Figures 4 and 5 and Figures S3, S4 (SI). It can be clearly seen that both Cd and S elements are uniformly distributed throughout the NWs. The distribution of the C and Pt elements also clearly support the presence of graphene sheets (Figs. 4 and S3) and the anchored Pt NPs on the surface of the NWs and rGO sheets (Figs. 4 and 5), respectively. Furthermore, larger Pt NPs with diameter 80-90 decorated onto graphene due to agglomeration of thin Pt NPs. In addition higher resolution elemental mapping and line scan also evidently show the uniform distribution of both Cd and S elements over the individual NWs (Figure 6). synergetic effect of CdS NWs in proposed nanocomposite toward ethanol oxidation increased. The UV-Vis spectra of CdS NWs and rGO/CdS NWs/Pt NPs nanocomposite are shown in Figure S5 A. As illustrated for CdS NWs, two absorption peaks are observed in 488 and 500 nm which is consistent with the previous reports.^{37,38} This observation indicates that the CdS NWs can successfully absorb blue and green wavelengths. For rGO/CdS NWs/Pt NPs nanocomposite, absorption intensity decreased, which originates from the presence of Pt NPs and rGO in the structure of nanocomposite. Figure S5 B and C presents the recorded photoluminescence spectra at excitation wavelengths of 403 and 488 nm, respectively, for both CdS NWs and rGO/CdS NWs/Pt NPs. As illustrated in Figure S5 B, under an excitation wavelength of 403 nm for CdS NWs, in agreement with the previous works,^{20,38} a sharp peak at 548 nm with two smaller peaks at 528 and 532 nm were observed. These peaks can be assigned

to near-band-edge emission and associated with structural defects that may arise from the excess of sulfur or defects on the nanowire surfaces.^{20,37,38} In the case of rGO/CdS NWs/Pt NPs, the same photoluminescence peaks, but with lower intensities, were observed. Since 488 nm was the observed absorption wavelength in the UV-Vis spectra of CdS NWs and rGO/CdS NWs/Pt NPs, the fluorescence spectra were also recorded at 488 nm as excitation wavelength. As can be seen in figure S5 C, two emission peaks are observable for CdS NWs in 518 and 528 nm. As well as for rGO/CdS NWs/Pt NPs, the same peaks were observed, but with less intensities. As previously reported, graphene do not display finite luminescence, but they are capable of quenching the photoluminescence of other photo display materials.³⁹ Therefore, reducing the fluorescence of rGO/CdS NWs/Pt NPs compared to CdS NWs can be due to the existence of graphene. It can be concluded from the herein UV-Vis and fluorescence data that CdS NWs and rGO/CdS NWs/Pt NPs can absorb the blue and green wavelengths of the visible electromagnetic radiation.

XPS was also employed to obtain more information about the oxidation state of platinum NPs and percentage of Pt in the nanocomposite. The XPS spectrum of rGO/CdS NWs/Pt NPs is shown in Figure 7. Apart from the cadmium, sulfur, carbon and oxygen bands, a distinct band is observed at binding energy (BE) of about 75 attributed to platinum. The percentage of Pt in the nanocomposite is calculated to be 1.96%. The recorded high resolution scan of Pt 4f peak (inset of Figure 7) reveals that this peak is a combination of two pairs of doublets. The most intense doublet (71.22 and 74.42 eV) is associated to metallic Pt and the analysis of peak area shows that 35% of Pt NPs was in metallic state (Pt⁰). The second set of doublets at BE of 72.92 and 76.22 eV can be attributed to Pt(II).^{12,13} These results clearly indicate that the Pt NPs successfully loaded on the surface of rGO and CdS NWs.

Electrocatalytic and Photoelectrocatalytic Oxidation of Ethanol in Alkaline Medium. The electrocatalytic oxidation of ethanol was carried out on glassy carbon electrodes modified with different nanocomposites including CdS NWs, rGO/Pt NPs, rGO/CdS NWs, CdS NWs/Pt NPs and rGO/CdS NWs/Pt NPs. The electrocatalytic activity of different nanocomposite based modified electrodes for oxidation of ethanol was investigated by recording CVs in aqueous solution of KOH (2.0 M), free or containing 3.0 M of C₂H₅OH, in the potential window of -1.1 to 0.3 V. Furthermore, the photo-assisted electrocatalytic oxidation of ethanol was also carried out at the same experimental condition under visible-light irradiation using a 1 W blue LED lamp as the illumination source. As can be seen in Figure 8A, voltammograms "a and b", when ethanol was absent, same redox response was observed for rGO/CdS NWs/Pt NPs in dark and under light irradiation. After adding ethanol to the alkaline solution (Figure 8A voltammogram "c"), a typical ethanol oxidation peak was observed at -0.38 V with the onset potential at -0.87 V vs Ag/AgCl. Surprisingly, after illumination with blue LED lamp, not only a three-fold increase was noticed in the current response, but also the onset potential shifted to -0.95 V (Figure 8A voltammogram "d"). The possible pathways for ethanol oxidation in dark and under visible light irradiation are shown in Scheme 2. As shown, different pathways are available for electron transfer under blue LED-light irradiation. To look into the influence of CdS NWs on electrocatalytic or photoelectrocatalytic activity of nanocomposite toward ethanol oxidation, the CV of GC electrode modified with rGO/Pt NPs is also shown (Figure 8B). As can be seen for this modified electrode, the onset and the peak potentials of ethanol oxidation were observed in -0.57 V and -0.25 V, respectively. The positive shift (0.30 V and 0.13 V in onset and peak potentials, respectively) on rGO/ Pt NPs compared to rGO/CdS NWs/Pt NPs nanocomposite clearly indicates the synergetic effect of CdS NWs toward ethanol oxidation especially under

light illumination. These results indicate adding of CdS NWs to rGO could greatly increase the surface areas available for Pt NPs and improving the catalytic activity of rGO/CdS NWs/Pt NPs compared to rGO/ Pt NPs. Furthermore, the decoration of rGO with CdS NWs decrease the aggregate of rGO back to the graphite structure is another factor which improved synergetic effect of CdS NWs in catalytic process. In addition due to photoactivity of CdS NWs under visible light irradiation the synergetic effect of CdS NWs in proposed nanocomposite toward ethanol oxidation increased.

Figure S6 presents the recorded CVs of GC electrode modified solely with CdS NWs in 2.0 M of KOH solution, free or containing 3.0 M ethanol. Obviously, there was no current response without ethanol in both situations of absence and presence of visible light irradiation. Ethanol addition also did not change the current response in dark condition, while under blue LED lamp irradiation, an increase in current was observed. This increase is related to the formation of electron-hole pairs in CdS and the presence of a reducing agent such as ethanol capable of donating electrons to the hole. As a result, ethanol can be oxidized by the holes that are formed during illumination. Indeed, under irradiation, the electrons transferred from valance band to the conduction band followed by transferring to the electrode, which led to increase in the current.^{19,39} Similar behavior has been reported for the oxidation of tyrosine by nanoporous TiO₂ in alkaline medium under irradiation with Xe lamp.⁴⁰

Continued control experiments using different modified electrodes further validate the much superior electrocatalytic or photoelectrocatalytic performance of toward ethanol oxidation. Figure 9 indicates the CVs of GC electrodes modified with CdS NWs, rGO/CdS NWs, CdS NWs/Pt NPs, rGO/Pt NPs and rGO/CdS NWs/Pt NPs in alkaline ethanol solution. As shown, no recognizable redox response was observed for CdS NWs, rGO/CdS NWs and CdS NWs/Pt NPs

modified electrodes, while rGO/Pt NPs modified electrode displayed a typical ethanol oxidation peak at -0.23 V with onset potential of -0.57 V and current density of 0.9 mA cm^{-2} . The electrocatalytic oxidation of alcohols on platinum nano-catalysts deposited on reduced graphene oxides have been reported.^{41,42}

These results clearly indicate that rGO plays a crucial role in improving the electrocatalytic activity of the nanocomposite toward ethanol oxidation by increasing surface conductivity as well as electron transfer kinetics. In the case of rGO/CdS NWs/Pt NPs modified electrode, the onset and peak potentials shifted to -0.870 and -0.38 V, respectively, and current density increased to 1.12 mA cm^{-2} . Under light irradiation, a yet further improvement was experienced in a way that the current density enhanced to 3.63 mA cm^{-2} and onset potential lowered to -0.95 V. This could be due to the synergism between the components (rGO, Pt NPs and CdS NWs) who dominate the electrocatalysis and photoelectrocatalysis phenomena during ethanol oxidation process. The current density, peak and onset potentials toward ethanol oxidation are summarized in Table 1 for different electrodes of rGO/Pt and rGO/CdS NWs/Pt NPs in dark and under light irradiation. The low onset potential and peak potential for rGO/CdS NWs/Pt NPs in both the dark and illuminated conditions signify the easy oxidation of ethanol at rGO/CdS NWs/Pt NPs modified electrode. Also, the high ratio of forward peak current density to backward peak current density (I_f/I_b) indicates a strong resistance against poisoning from intermediates generated during the electrooxidation of ethanol.^{9,14} Table 2 lists the various characteristic parameters of our proposed nanocomposite and some other systems reported in literature. As is obvious, the herein obtained data for ethanol oxidation in alkaline media are better in some cases or comparable with reported values of other Pt catalysis-based works.

Further evidence for improved electron transfer kinetics of rGO/CdS NWs/Pt NPs nanocomposite was provided by CV and EIS experiments using $\text{Fe}(\text{CN})_6^{4-/3-}$ as redox probe (Figure 10). As shown, in the case of rGO/CdS NWs/Pt NPs, the redox response increased and peak potential separation decreased in recorded voltammograms, while charge transfer resistance (R_{ct}) in EIS measurement was dramatically decreased. Indeed, the presence of rGO in nanocomposite structure efficiently facilitated its electron transfer characteristics.

The transient photocurrent response is commonly employed to evaluate the separation of photoinduced electron-hole pairs, because the transfer of photogenerated charge carriers is the key factor determining the overall photoactivity associated with semiconductor based materials.^{1,19} Figure 11 A shows the cyclic “ON” and “OFF” formation of light-induced photocurrents at the rGO/CdS NWs/Pt NPs electrode as current-time (I-t) curves during periodically light irradiations. Apparently, under visible light illumination, the photocurrent response rapidly increases up to a value of 1.12 mA cm^{-2} and then it comes back to its original value of 0.23 mA cm^{-2} with turning the light off again. This observation confirms that an effective separation of photogenerated electron-hole pairs occurs at rGO/CdS NWs/Pt NPs electrode. This manner can also be observed at other modified electrodes of CdS NWs, rGO/CdS NWs and CdS NWs/Pt NPs with the difference that in these latter cases, the photocurrent increase is much lower than that obtained for rGO/CdS NWs/Pt NPs. Notably, the transient photocurrent responses were highly reproducible observed for all the studied electrodes over several on-off cycles of intermittent visible light illumination. These results indicated the diffusion of the photogenerated electrons to the back contact originates photocurrent and the photoinduced holes are taken by ethanol as acceptor. Accordingly, the photocurrent of rGO/CdS NWs/Pt NPs electrode is approximately 9.4, 7.74 and 5.56 times higher than that of CdS NWs,

rGO/CdS NWs and CdS NWs/Pt NPs electrodes, respectively. This significantly demonstrates the more efficient separation and longer life time of photoexcited electron-hole pairs of ternary hybrid rGO/CdS NWs/Pt NPs than each of CdS NWs, rGO/CdS NWs and CdS NWs/Pt NPs modified electrodes.

The long-term stability is another important factor for a catalyst to be considered in various practical applications. To evaluate the stability of the proposed catalyst, chronoamperometric measurements were performed in 2.0 M KOH containing 3.0 M ethanol. Figure 11 B shows I-t plots for ethanol oxidation measured at a fix potential of -0.32 V during 3500 s for rGO/CdS NWs/Pt NPs modified electrode in dark and under visible light irradiation. As illustrated, the maximum initial and steady-state oxidation current densities are evidently larger upon illumination, indicating the catalytic activity and stability are improved and photoassisted electrocatalytic process could remarkably enhance the oxidation efficiency toward ethanol oxidation.

CONCLUSION

In conclusion, a ternary rGO/CdS NWs/Pt NPs nanocomposite is successfully synthesized via a template-free route. The novel nanohybrid material combines the excellent electrocatalytic properties of Pt nanoparticles and amazing photocatalytic features of 1D CdS NWs with the unique and attractive electronic behavior of rGO nanosheets. Through different microscopic and spectroscopic techniques employed for characterizing the morphology and characteristics of nanohybrid, the successful modification of rGO with uniformly sized CdS NWs having diameters of 35 nm and decorated with Pt NPs has been demonstrated. CV and amperometry measurements indicated the excellent electrocatalytic activity of ternary nanocomposite toward ethanol oxidation in alkaline media and interestingly, under visible light irradiation using a low

power blue LED lamp, the current density dramatically increased and the onset potential underwent a negative shift to -0.95 V due to efficiently enhanced lifetime and faster interfacial charge transfer rate. In addition, over several on-off cycles of intermittent visible light illumination, transient photocurrent responses with good reproducibility were observed for rGO/CdS NWs/Pt NPs electrodes. Low onset potential, high ratio of I_f/I_b , low percentage of Pt (1.96%) in nanocomposite and low power radiation source are the main advantages of the proposed composite. The ternary rGO/CdS NWs/Pt NPs may find promising potential applications in high efficient and stable anode for fuel cell and photoanode in photoactivated fuel cells or other related fields.

ASSOCIATED CONTENT

Supporting Information

The images of CdS NWs and rGO/CdS NWs/Pt NPs nanocomposite. The EDX and HRTEM for rGO/CdS NWs/Pt NPs nanocomposite. UV-Vis, fluorescence spectra and the CV for GC electrode modified with rGO/CdS NWs/Pt NPs and CdS NWs.

AUTHOR INFORMATION

Corresponding Author

* Email: absalimi@uok.ac.ir , absalimi@yahoo.com (A.Salimi). Tel.: +98 87 33624001; Fax: +98 87 33624001

ACKNOWLEDGMENTS

The financial supports of the Iranian Nanotechnology Initiative and Research Office of University of Kurdistan are gratefully acknowledged. We thanks Dr. Hazhir Teymourian for his valuable comments.

REFERENCES

- 1 C. Zhai, M. Zhu, D. Bin, H. Wang, Y. Du, C. Wang and P. Yang, *ACS Appl. Mater. Interfaces*, 2014, **6**, 17753-17761.
- 2 Y. S. Li, T. S. Zhao and Z. X. Liang, *J. Power Sources*, 2009, **187**, 387-392.
- 3 W. Du, Q. Wang, D. Saxner, N. A. Deskins, D. Su, J. E. Krzanowski, A. I. Frenkel and X. Teng, *J. Am. Chem. Soc.*, 2011, **133**, 15172-15183.
- 4 W. Du, G. Yang, E. Wong, N. A. Deskins, A. I. Frenkel, D. Su and X. Teng, *J. Am. Chem. Soc.* 2014, **136**, 10862-10865.
- 5 S. Y. Shen, T. S. Zhao, J. B. Xu and Y. S. Li, *J. Power Sources*, 2010, **195**, 1001-1006.
- 6 F. Ren, H. Wang, C. Zhai, M. Zhu, R. Yue, Y. Du, P. Yang, J. Xu and W. Lu., *ACS Appl. Mater. Interfaces*, 2014, **6**, 3607-3614.
- 7 W. Hong, J. Wang and E. Wang, *ACS Appl. Mater. Interfaces*, 2014, **6**, 9481-9487.
- 8 R. Yue, H. Wang, D. Bin, J. Xu, Y. Du, W. Lu and J. Guo, *J. Mater. Chem. A*, 2015, **3**, 1077-1088.
- 9 A. Dutta and J. Ouyang, *ACS Catal.*, 2015, **5**, 1371-1380.
- 10 C. Wang, H. Wang, C. Zhai, F. Ren, M. Zhu, P. Yang and Y Du, *J. Mater. Chem. A*, 2015, **3**, 4389-4398.
- 11 M. Wang, X. Song, Q. Yang, H. Hua, S. Dai, C. Hu and D. Wei, *J. Power Sources*, 2015, **273**, 624-630.
- 12 Y. Shen, K. Xiao, J. Xi and X. Qiu, *J. Power Sources*, 2015, **278**, 235-244.
- 13 A. Navaee, A. Salimi and S. Soltanian, *J. Power Sources*, 2015, **277**, 268-276.
- 14 X. Yang, Q. Yang, J. Xu and C. S. Lee, *J. Mater. Chem.*, 2012, **22**, 8057-8062.
- 15 H. Gao, F. Xiao, C. B. Ching and H. Duan, *ACS Appl. Mater. Interfaces*, 2011, **3**, 3049-3057.
- 16 H. Teymourian, A. Salimi and S. Khezrian, *Biosens. Bioelectron.*, 2013, **49**, 1-8.

- 17 Y. X. Huang, J. F. Xie, X. Zhang, L. Xiong and H. Q. Yu, *ACS Appl. Mater. Interfaces*, 2014, **6**, 15795-15801.
- 18 Y. Zhu, Y. Wang, Z. Chen, L. Qin, L. Yang, L. Zhu, P. Tang, T. Gao, Y. Huang, Z. Sha and G. Tang, *Appl Catal., A Gen.*, 2015, **498**, 159-166.
- 19 S. Liu, Z. Chen, N. Zhang, Z. R. Tang and Y. J. Xu, *J. Phys. Chem. C*, 2013, **117**, 8251-8261.
- 20 S. Liu, N. Zhang, Z. R. Tang and Y. J. Xu, *ACS Appl. Mater. Interfaces*, 2012, **4**, 6378-6385.
- 21 N. Qin, Y. Liu, W. Wu, L. Shen, X. Chen, Z. Li and L. Wu, *Langmuir*, 2015, **31**, 1203-1209.
- 22 N. Zhang, Y. Zhang, X. Pan, X. Fu, S. Liu and Y. Xu, *J. Phys. Chem. C*, 2011, **115**, 23501-23511.
- 23 Z. R. Tang, X. Yin, Y. Zhang and Y. J. Xu, *Inorg. Chem.*, 2013, **52**, 11758-11766.
- 24 P. Pathak, S. Gupta, K. Grosulak, H. Imahori and V. Subramanian, *J. Phys. Chem. C*, 2015, **119**, 7543-7553.
- 25 T. T. Xuan, J. Q. Liu, R. J. Xie, H. L. Li and Z. Sun, *Chem. Mater.*, 2015, **27**, 1187-1193.
- 26 C. J. Lin, L. C. Kao, Y. Huang, M. A. Banares and S. Y. H. Liou, *Int. J. Hydrogen Energ.*, 2015, **40**, 1388-1393.
- 27 R. Zhou, Q. Zhang, E. Uchaker, J. Lan, M. Yin and G. Cao, *J. Mater. Chem. A*, 2014, **2**, 2517-2525.
- 28 M. J. Speirs, D. M. Balazs, H. H. Fang and L. H. Lai, *J. Mater. Chem. A*, 2015, **3**, 1450-1457.
- 29 H. Park, H. H. Ou, A. J. Colussi and M. R. Hoffmann, *J. Phys. Chem. A*, 2015, DOI: 10.1021/jp511329d.
- 30 M. Antoniadou, D. I. Kondarides, D. D. Dionysiou and P. Lianos, *J. Phys. Chem. C*, 2012, **116**, 16901-16909.
- 31 J. Zheng, X. Xue, D. Lia and Y. Zhao, *CrystEngComm.*, 2015, **17**, 1509-1512.
- 32 P. Gao, J. Liu, S. Lee, T. Zhang and D. D. Sun, *J. Mater. Chem.*, 2012, **22**, 2292-2298.

- 33 S. Perera, R. Mariano, K. Vu, N. Nour, O. Seitz, Y. Chabal and J. K. J. Balkus, *ACS Catal.*, 2012, **2**, 949-956.
- 34 L. Wang, H. Wei, Y. Fan, X. Gu and J. Zhan, *J. Phys. Chem. C*, 2009, **113**, 14119-14125.
- 35 Z. Gao, N. Liu, D. Wu, W. Tao, F. Xu and K. Jiang, *Appl. Surf. Sci.*, 2012, **258**, 2473- 2478.
- 36 N. Zhang, Y. Zhang, X. Pan, M. Q. Yang and Y. J. Xu, *J. Phys. Chem. C*, 2012, **116**, 18023-18031.
- 37 D. Xu, Z. Liu, J. Liang and Y. Qian, *J. Phys. Chem. B*, 2005, **109**, 14344-14349.
- 38 Y. Li, H. Liao, Y. Ding, Y. Fan, Y. Zhang and Y. Qian, *Inorg. Chem.*, 1999, **38**, 1382-1387.
- 39 K. P. Loh, Q. Bao, G. Eda and M. Chhowalla, *Nature Chem.*, 2010, **2**, 1015-1024.
- 40 M. Kaneko, S. Suzuki, H. Ueno, J. Nemoto and Y. Fujii, *Electrochim. Acta*, 2010, **55**, 3068-3074.
- 41 F. Li, Y. Guo, T. Wu, Y. Liu, W. Wang, J. Gao, *Electrochim. Acta*, 2013, **111**, 614– 620.
- 42 F. Li, Y. Guo, M. Chen, H. Qiu, X. Sun, W. Wang, Y. Liu, J. Gao, *Int. J. Hydrogen Ener.*, 2013, **38**, 14242-14249.
- 43 H. Hua, C. Hu, Z. Zhao, H. Liu, X. Xie and Y. Xi, *Electrochim. Acta*, 2013, **105**, 130-136.
- 44 X. Chen, Z. Cai, X. Chen and M. Oyamac, *J. Mater. Chem. A*, 2014, **2**, 315-320.
- 45 S. Y. Shen, T. S. Zhao and J. B. Xu, *Int. J. Hydrogen Ener.*, 2010, **35**, 12911-12917.
- 46 J. J. Lv, N. Wisitruangsakul, J. J. Feng, J. Luo, K. M. Fang and A. J. Wang, *Electrochim. Acta*, 2015, **160**, 100-107.
- 47 K. Ding, Y. Zhao, L. Liu, Y. Cao, Q. Wang, H. Gu, X. Yan and Z. Guo, *Int. J. Hydrogen Ener.*, 2014, **39**, 17622-17633.

Figure Captions

Table 1. Catalytic Performance Characteristics of rGO/CdS NWs/Pt NPs and rGO/Pt NPs Nanocomposites for Ethanol Electrooxidation in Alkaline Medium

Table 2. Peak Potential, Onset Potential and the ratio of I_f to I_b for the Pt and Pt-Based Catalyst Electrodes for Ethanol Oxidation in Alkaline Media

Scheme 1. Schematic flowchart for two-step synthesis of rGO/CdS NWs/Pt NPs.

Scheme 2. Schematic illustration for photoassisted electrocatalytic oxidation of ethanol by using rGO/CdS NWs/Pt NPs electrode under blue LED-light irradiation. A, B and C are the possible pathways of electron transfer in the presence of blue LED-light irradiation and A is possible pathway of electron transfer in the absence of irradiation.

Figure 1. SEM images of (A), (B) CdS NWs and (C), (D) and (E) rGO/CdS NWs/Pt NPs nanocomposite

Figure 2. XRD patterns of CdS NWs (blue line) and rGO/CdS NWs/Pt NPs (green line) nanocomposites.

Figure 3. The HRTEM images (A-C) and HRTEM images corresponding SAED patterns (D) for individual NWs selected from rGO/CdS NWs/Pt NPs nanocomposite.

Figure 4. The HRTEM with low magnification and the elemental mapping results for rGO/CdS NWs/Pt NPs nanocomposite.

Figure 5. The HRTEM with high magnification and the elemental mapping results for rGO/CdS NWs/Pt NPs nanocomposite.

Figure 6. The HRTEM elemental mapping and line scan for individual NWs in rGO/CdS NWs/Pt NPs nanocomposite.

Figure 7. XPS survey spectra of rGO/CdS NWs/Pt NPs. Insert illustrate the high resolution scans of corresponding Pt 4f XPS spectra.

Figure 8. (A) CV for GC electrode modified with rGO/CdS NWs/Pt NPs, (a) and (b) in 2.0 M KOH at scan rate of 50 mV s^{-1} without blue LED light irradiation and with blue LED light irradiation, respectively. (c) and (d) as (a) and (b) in presence of 3.0 M $\text{C}_2\text{H}_5\text{OH}$ without blue LED light irradiation and with blue LED light irradiation, respectively. The onset potential is shown in the insert. (B) CV for GC electrode modified with rGO/Pt NPs, pink line is in 2.0 M KOH at scan rate of 50 mV s^{-1} and blue line is in the presence of 3.0 M ethanol.

Figure 9. CVs of (a) CdS NWs, (b) rGO/CdS NWs, (c) CdS NWs/Pt NPs, (d) rGO/Pt NPs and (e) rGO/CdS NWs/Pt NPs electrode in dark and (f) under blue LED light irradiation in $\text{C}_2\text{H}_5\text{OH}$ (3.0 M) and KOH (2.0 M) solution at a scan rate of 50 mV s^{-1} .

Figure 10. CVs of (A) CdS NWs (black line), CdS NWs/Pt NPs (red line), rGO/CdS NWs (green line) and rGO/CdS NWs/Pt NPs electrode (blue line) in $3.0 \text{ mM } [\text{Fe}(\text{CN})_6]^{-3/4}$ and 0.1 M KCl at a scan rate of 50 mV s^{-1} . (B) EIS Nyquist spectra of CdS NWs (black line), CdS NWs/Pt NPs (red line), rGO/CdS NWs (green line) and rGO/CdS NWs/Pt NPs electrode (blue line) in $3.0 \text{ mM } [\text{Fe}(\text{CN})_6]^{-3/4}$ and 0.1 M KCl . Frequency range and applied potential for recorded plots were 0.1 Hz to 10 kHz and 0.22 V , respectively.

Figure 11. (A) Photocurrent responses of rGO/CdS NWs/Pt NPs electrode and CdS NWs (black line), rGO/CdS NWs (green line) and CdS NWs/Pt NPs (red line) electrodes under light irradiation in $3.0 \text{ M } \text{C}_2\text{H}_5\text{OH}$ and 2.0 M KOH solution recorded at -0.32 V vs Ag/AgCl. The illumination from a blue LED lamp was interrupted every 30 s. (B) Chronoamperometric curves of rGO/CdS NWs/Pt NPs electrode without blue LED light irradiation (red line) and with blue LED light irradiation in $3.0 \text{ M } \text{C}_2\text{H}_5\text{OH}$ and 2.0 M KOH for 3500 s at -0.32 V vs Ag/AgCl.

Table 1. Catalytic Performance Characteristics of rGO/CdS NWs/Pt NPs and rGO/Pt NPs Nanocomposites for Ethanol Electrooxidation in Alkaline Medium

Electrode	Peak potential (V)	Onset potential (V)	I_f (mA cm ⁻²)	I_b (mA cm ⁻²)	I_f/I_b
rGO/CdS NWs/Pt NPs (without ligh)	-0.38	-0.87	1.12	0.51	2.19
rGO/CdS NWs/Pt NPs (with ligh)	-0.32	-0.95	3.63	1.70	2.14
rGO/Pt NPs	-0.23	-0.57	0.94	0.35	2.68

Table 2. Peak Potential, Onset Potential and the ratio of I_f to I_b for the Pt and Pt-Based Catalyst Electrodes for Ethanol Oxidation in Alkaline Media

Catalyst electrodes	Peak potential (V)	Onset potential (V)	I_f/I_b	Solution	
Pt/G3DN ^a	-0.27*	-	0.65	1 M EtOH + 1 M KOH	11
Pt/N-Gr ^b	~-0.050*	-0.67*	1.15	1 M EtOH + 0.1 M KOH	13
Pt/TiO ₂	-0.22*	-	0.99	1 M EtOH + 1 M KOH	43
PtPd NPs/GNs ^c	-0.24*	-0.64*	~1.8	1 M EtOH + 1 M NaOH	44
Pt ₂ Rh/C ^d	-0.08***	-0.55***	1.9	1 M EtOH + 1 M KOH	45
PtPd alloyed	~-0.30**	~-0.65**	2.23	1 M EtOH + 0.5 M KOH	46
PtNi ₃ /MWNTs	~-0.28**	-0.67**	1.12	1 M EtOH + 1 M KOH	47
rGO/CdS NWs/Pt NPs (without light)	-0.38*	-0.87*	2.19	3 M EtOH + 2 M KOH	This work
rGO/CdS NWs/Pt NPs (with light)	-0.32*	-0.95	2.14		

*Potential vs Ag/AgCl

**Potential vs SCE

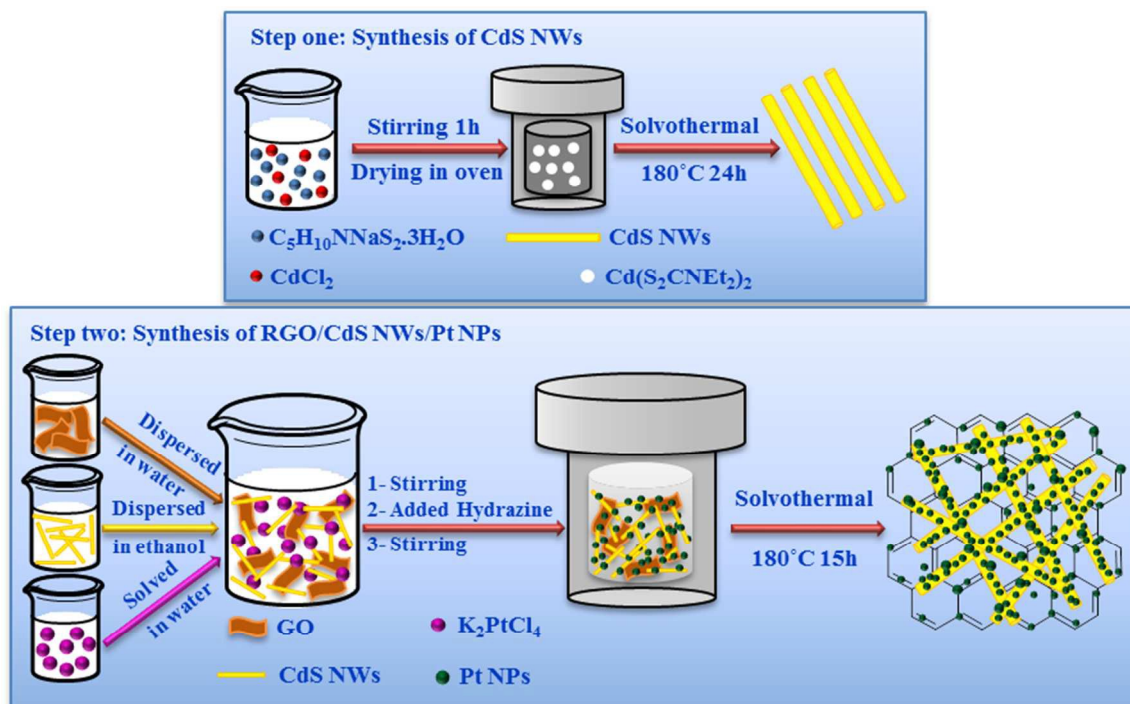
***Potential vs Hg/HgO

a= Pt/ graphene three-dimensional network

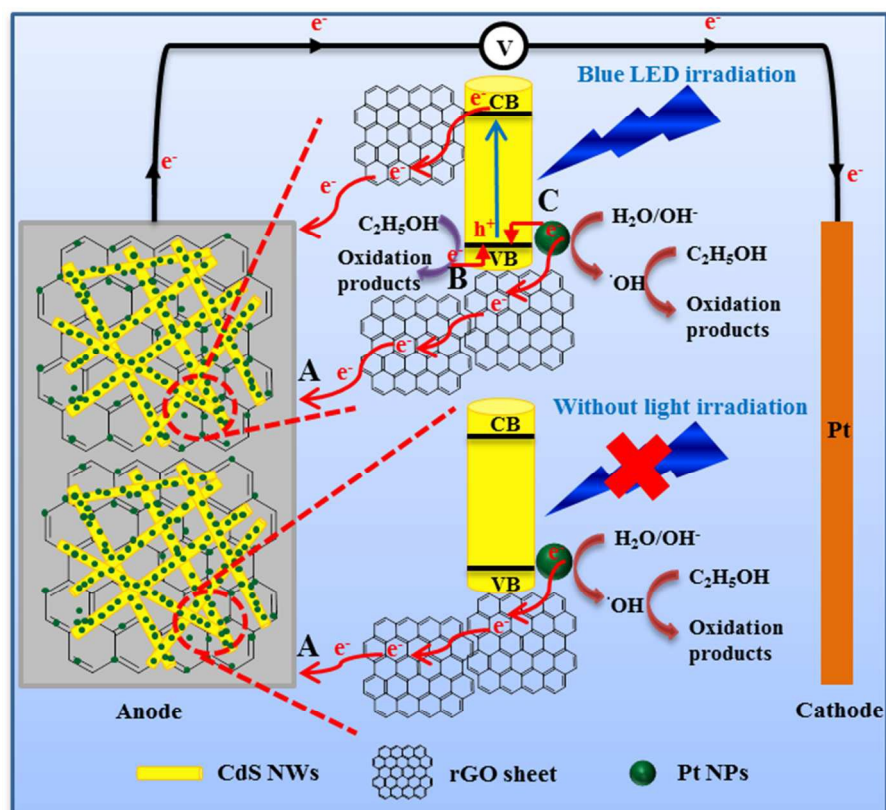
b= Pt/ nitrogen doped graphene

c= PtPd alloy nanoparticles/ grapheme nanosheets

d= Carbon supported PtRh



Scheme 1



Scheme 2

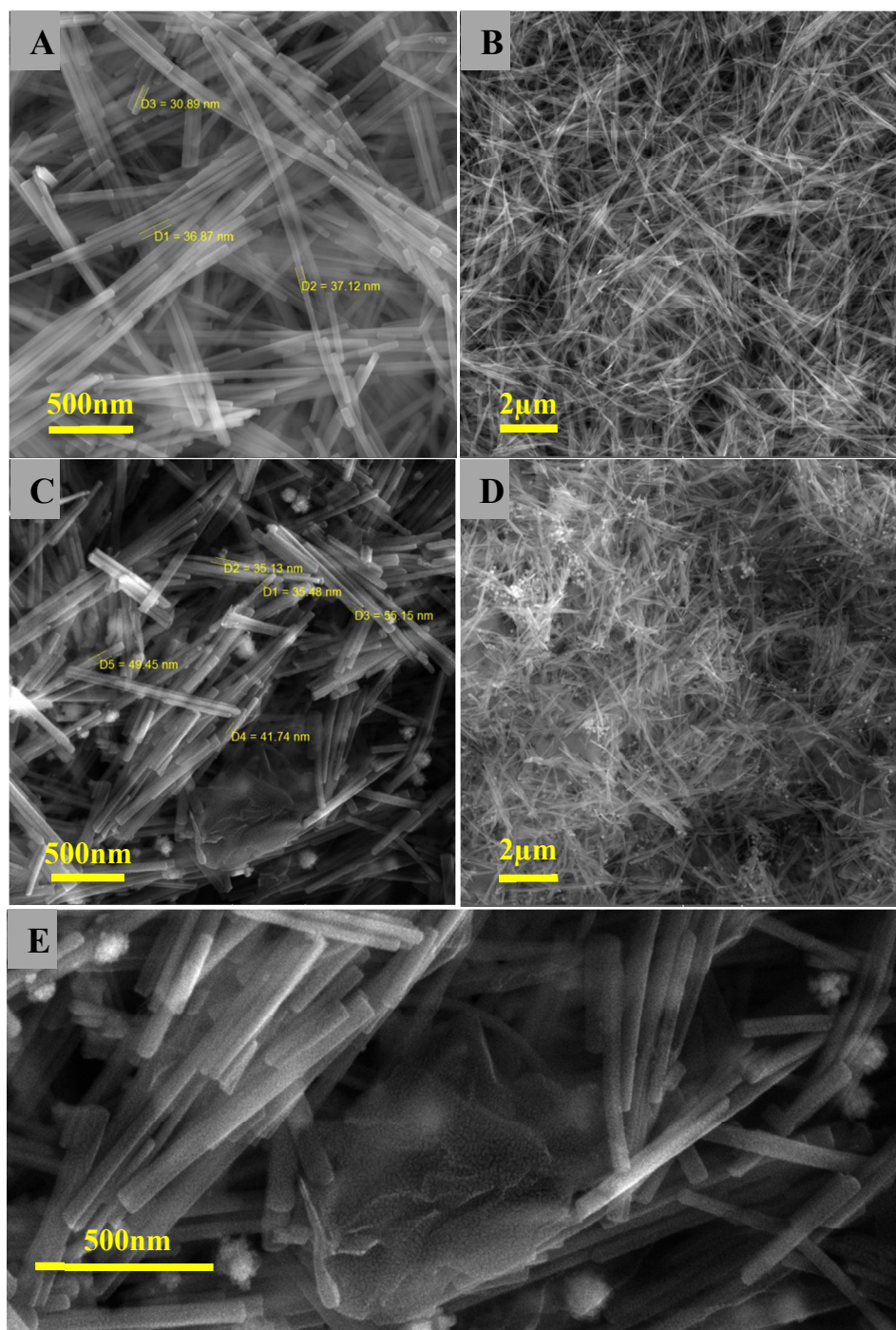


Figure 1

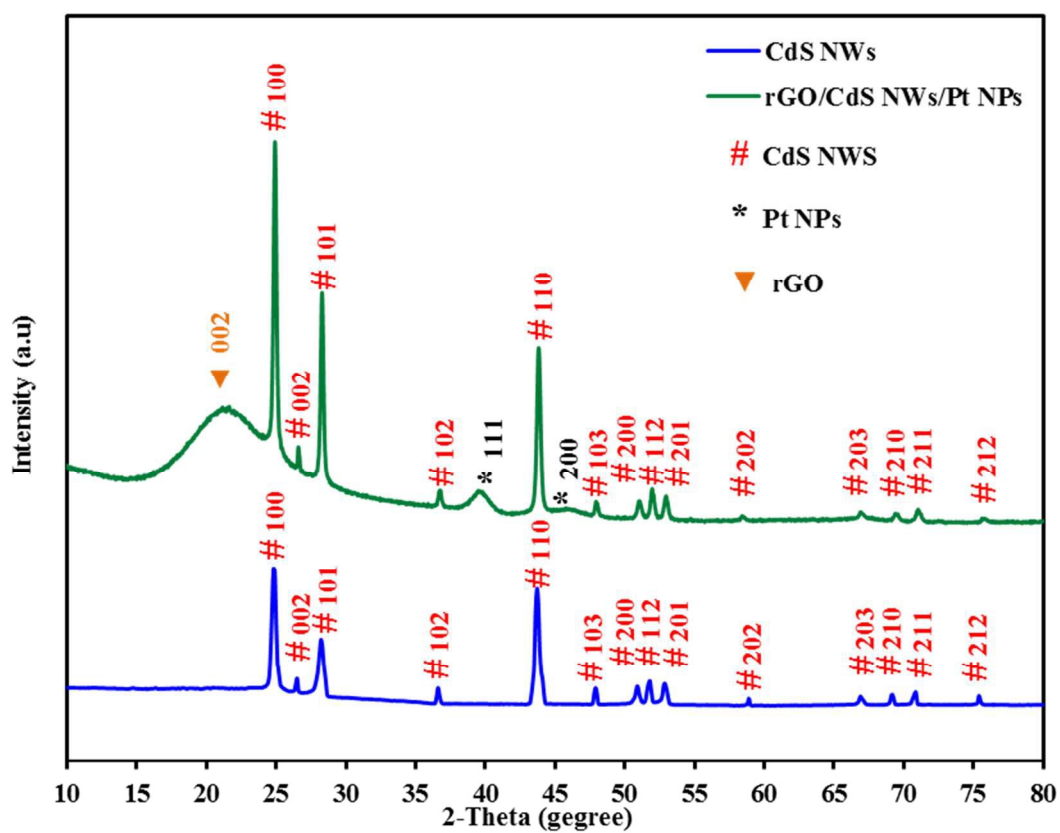


Figure 2

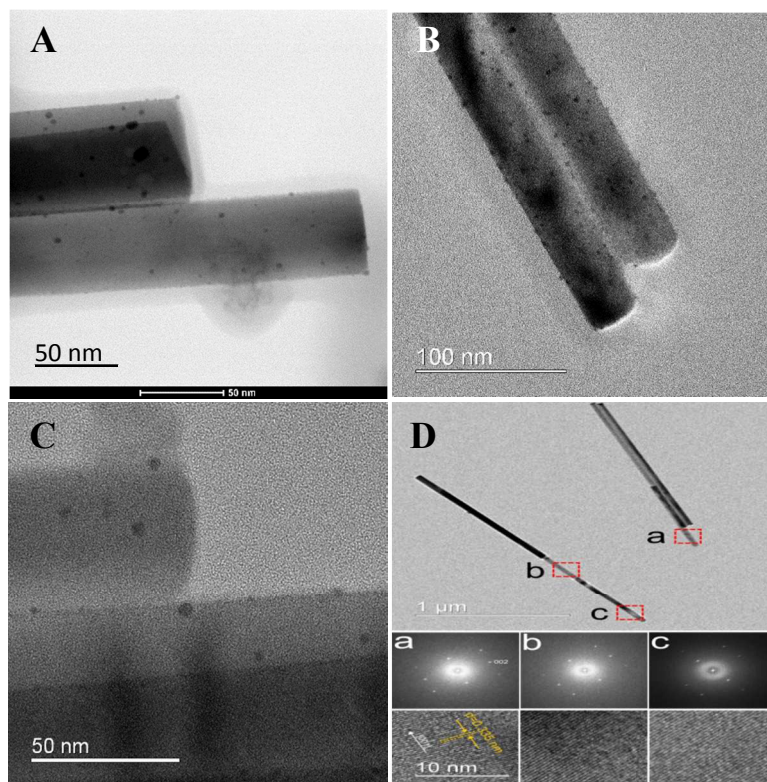


Figure 3

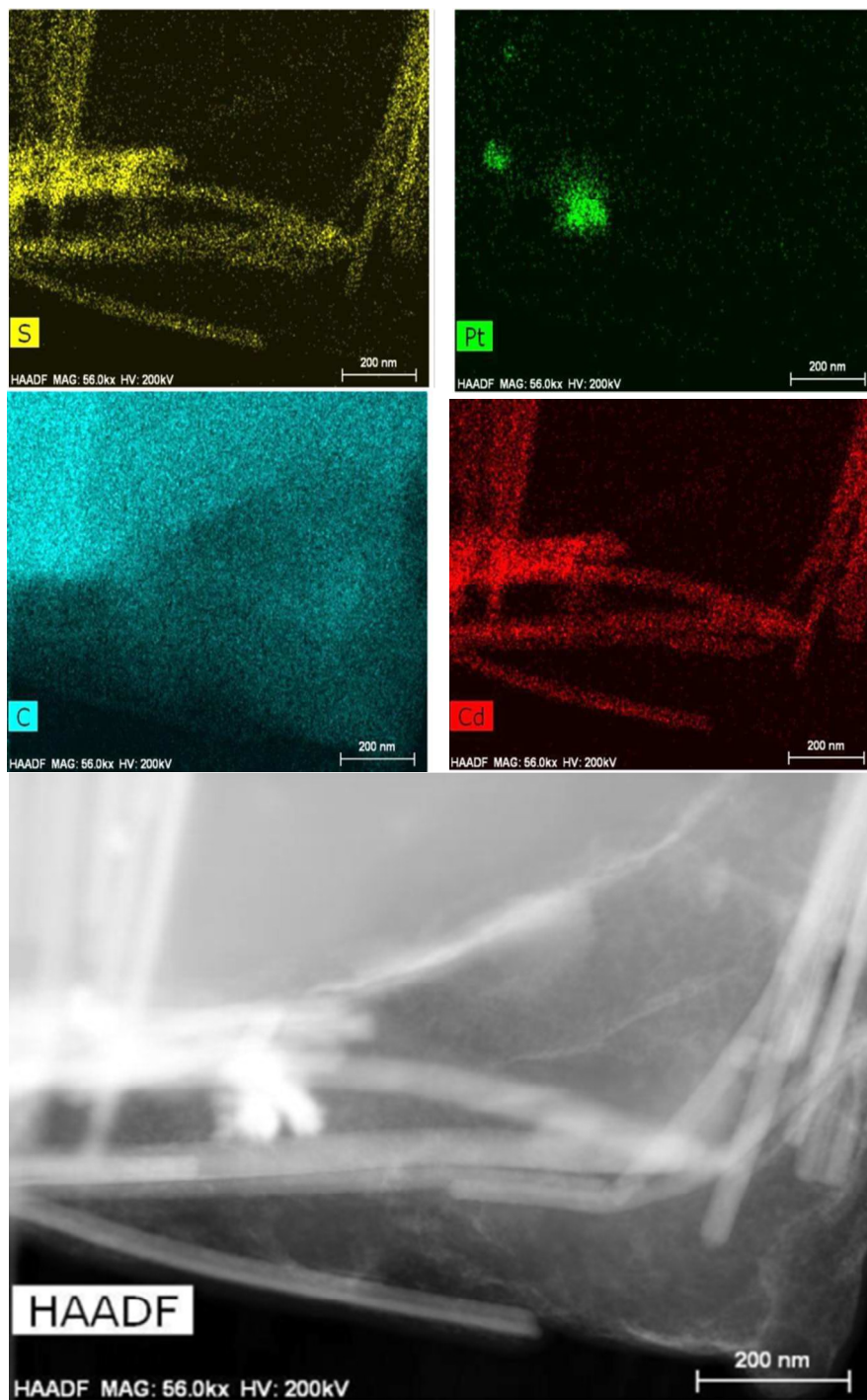


Figure 4

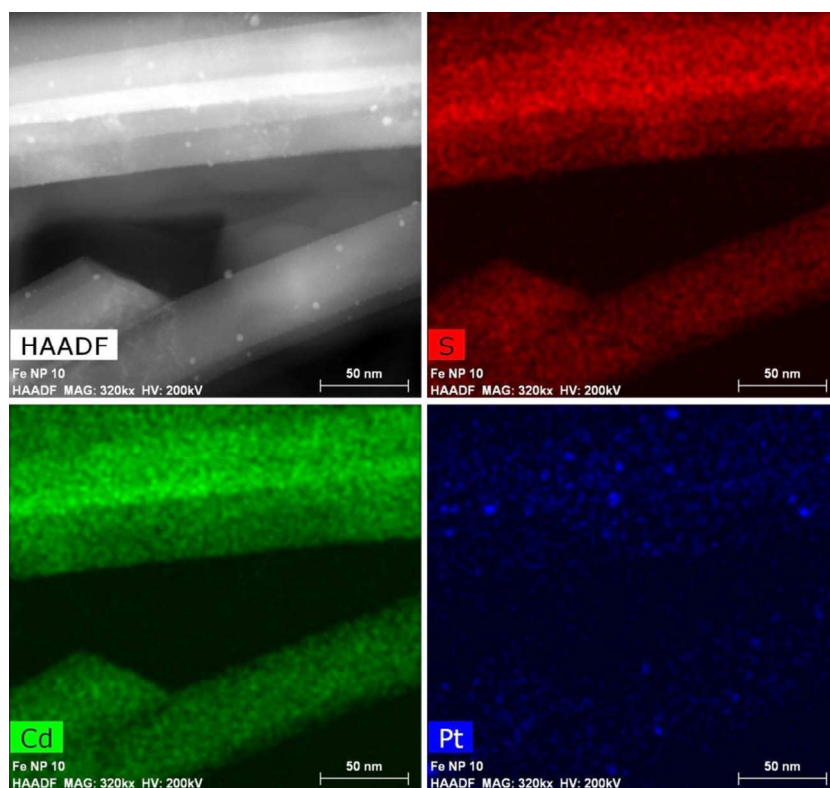


Figure 5

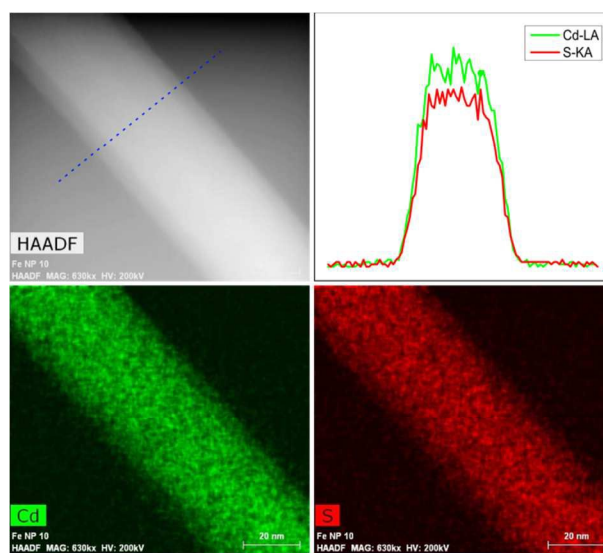


Figure 6

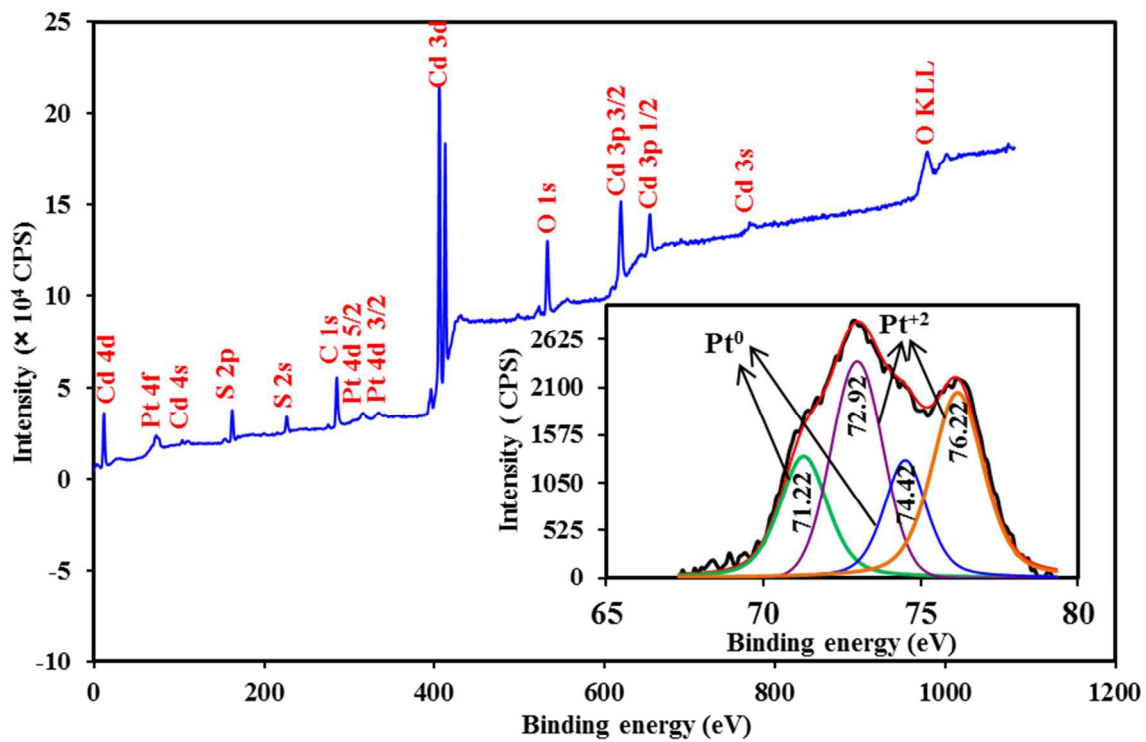


Figure 7

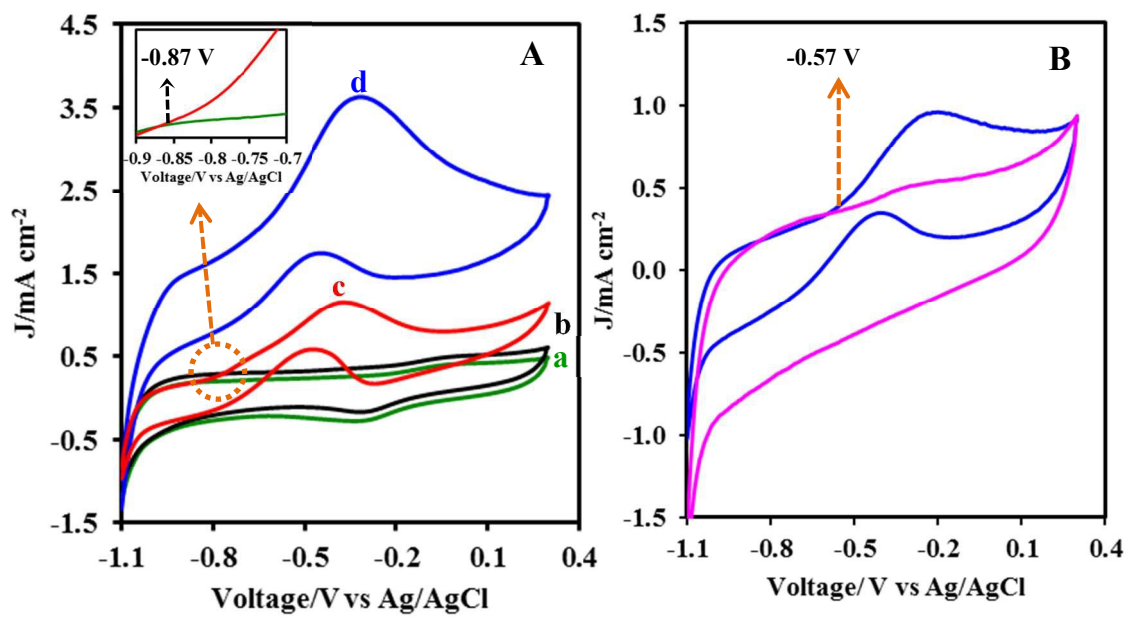


Figure 8

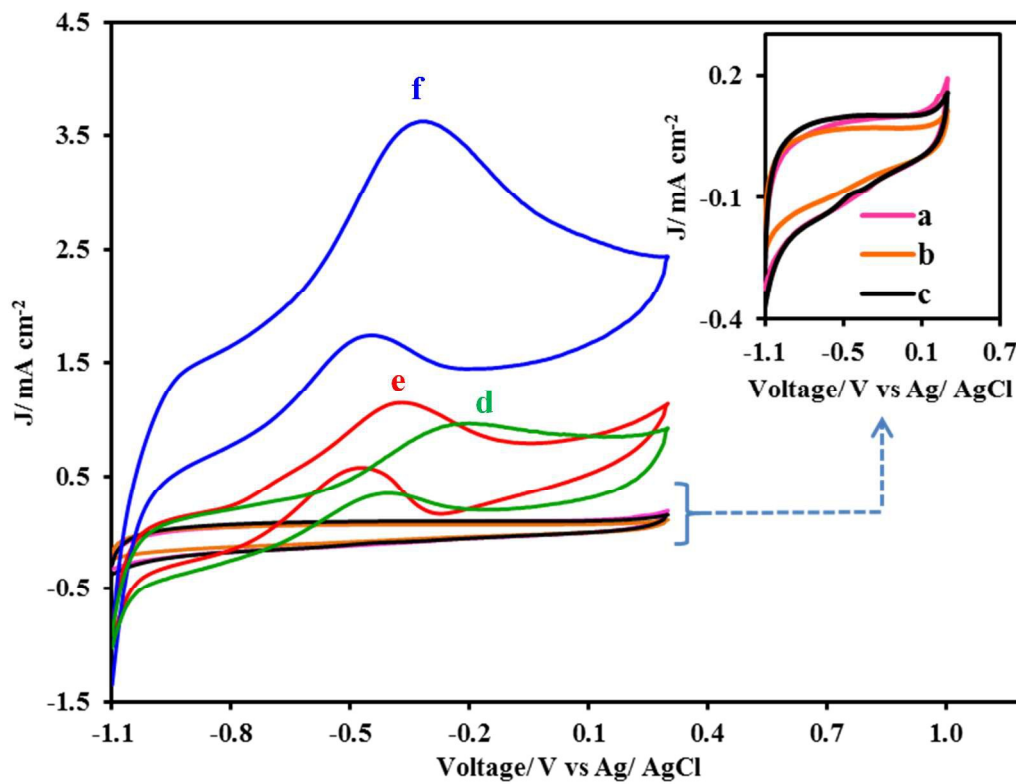


Figure 9

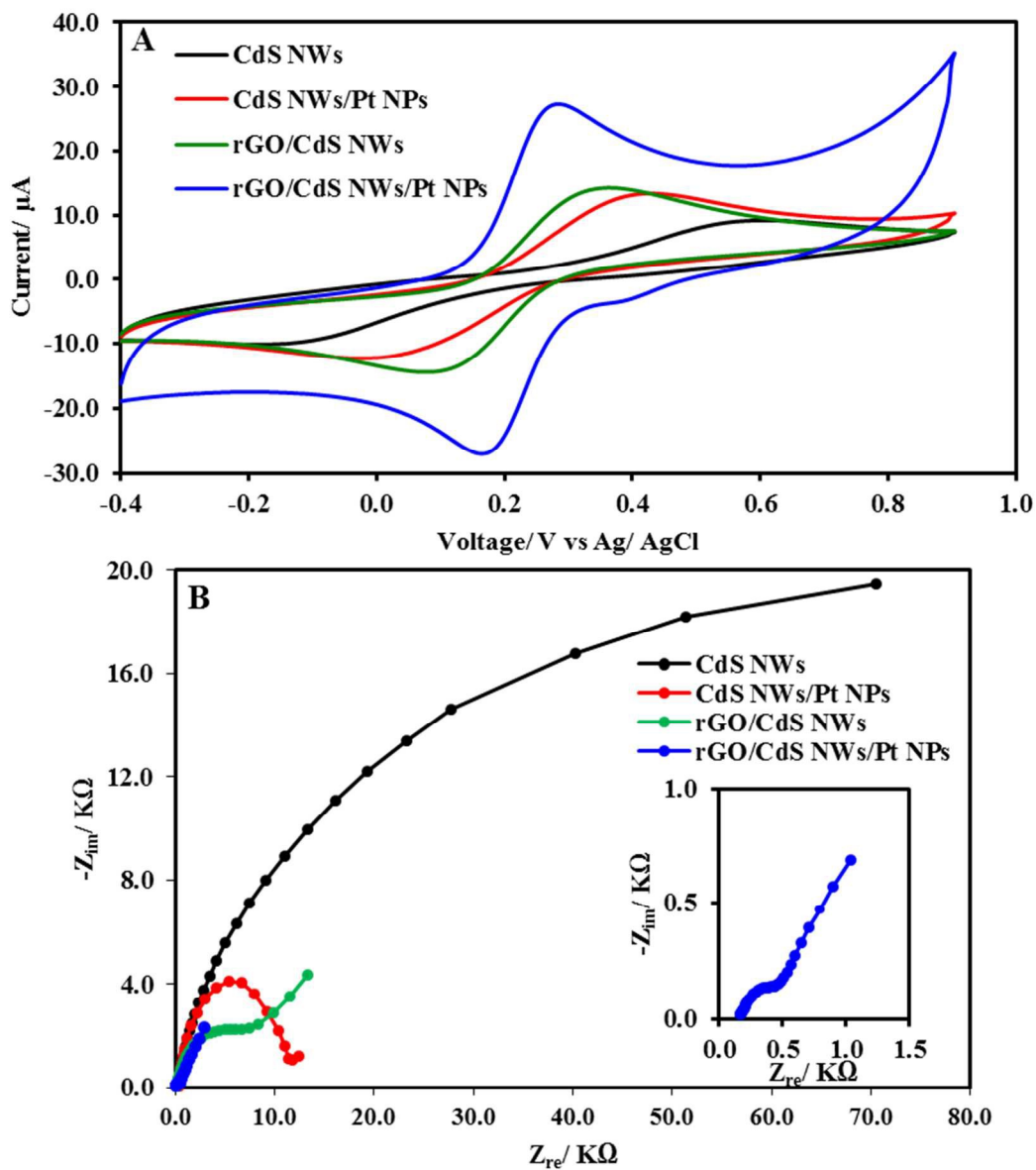


Figure 10

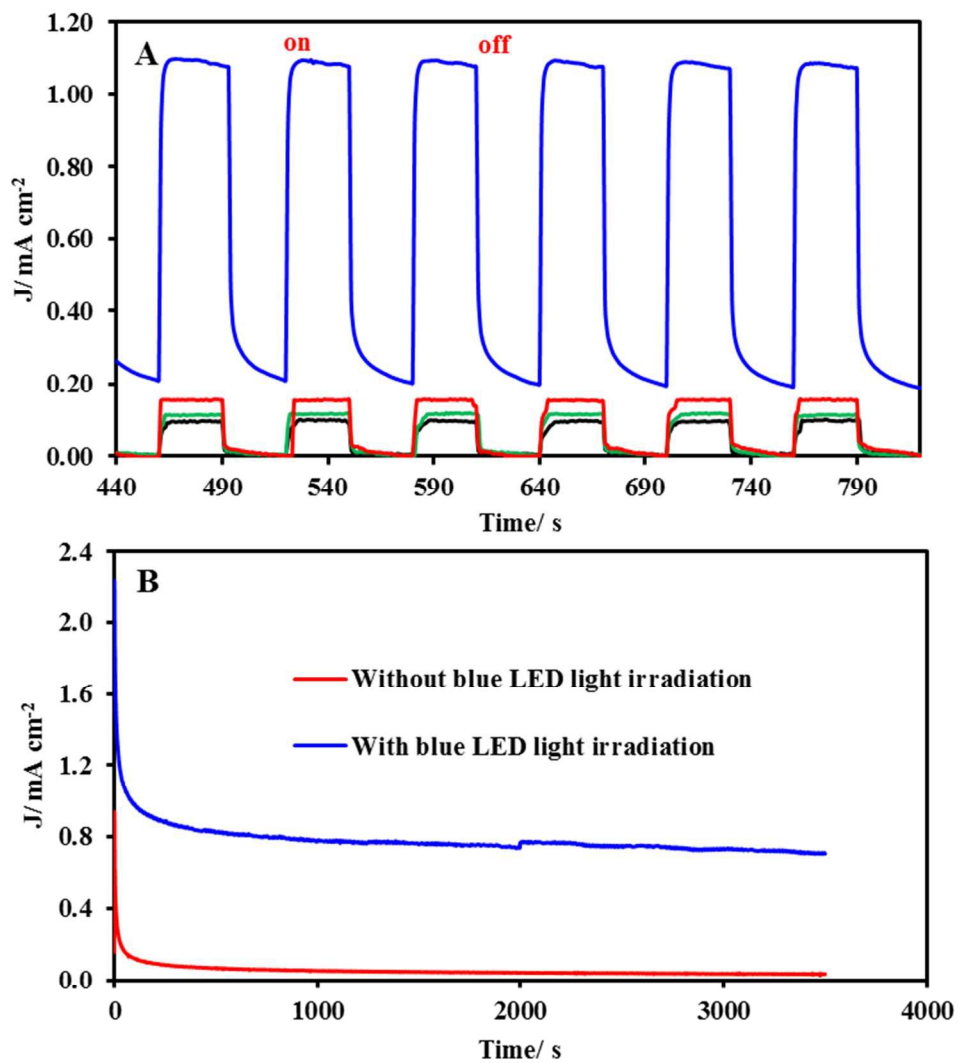


Figure 11

Graphical Abstract

A ternary rGO/CdS NWs/Pt NPs nanocomposite is successfully synthesized via a template-free route and its application for electrocatalytic and photoelectrocatalytic oxidation of ethanol was developed.

